Imed Jlassi[1], Sejir Khojet El Khil[2]

J. Electrical Systems 10-1 (2014): 48-62

Regular paper

A MRAS-Luenberger Observer Based Fault Tolerant Control of PMSM Drive

This paper presents a fault tolerant control FTC strategy of Permanent Magnet Synchronous Motor PMSM drive. Position sensor fault detection, isolation and reconfiguration are presented for control scheme devoted for PMSM. MRAS estimator and Luenberger observer are used in order to generate residuals for detection the defect, and then the estimator is used to reconfigure the drive and to conserve the performances of system in order to increase the reliability and to ensure the continuity of the process. The validity of the proposed strategy has been verified by the simulation.

Keywords: Permanent-Magnet Synchronous Motor (PMSM), position sensor failure, fault tolerant control (FTC), MRAS estimator and Luenberger observer

1. Introduction

Availability and continuity of service of electric drives with variable speed contribute mainly to the increasing performance and minimizing downtime. The variable speed electric drives using the Permanent Magnet Synchronous Motors PMSM are becoming more attractive for various applications such as electric vehicles [1] or electric traction railway [2]. For these applications, the detection of a fault and fault tolerance control contribute primarily to the availability, reliability and reduced downtime of the process.

Several studies have focused on fault detection and fault tolerant controls for synchronous machines. But these studies have focused most of them on the defects in semiconductor converters or defects of inductances of the machine. Although the information and statistics on the sensor faults are not always available, it is clear that in the case of a sensor failure, a shutdown of the system is necessary. Fault detection of sensors and reconfiguration drives has earned attention [3]. In [4] a specific controller architecture based on two virtual sensors (a two-stage extended Kalman filter and a back-electromotive-force adaptative observer) is dedicated to obtain a PMSM drive that is robust to speed sensor failure. Fault detection of position sensor algorithms based on wavelet decomposition and especially multiresolution analyses technique, and parity equations method are compared in [5]. Sensor fault-tolerant control for electric vehicles has also been treated in [6], [7], [8] and [9]. Fuzzy methods are used have been used [10] to reconfigure a drive for an induction motor. In [11], [12] and [13] observer and estimator based methods have been investigated for fault tolerant control FTC dedicated for Doubly-Fed Induction Generator DFIG. In [14] the discrete wavelet transform is used for fault tolerant control of induction motor.

In this work, the aim is to propose a strategy for fault tolerant control position sensor to detect and isolate a defect and then reconfigure the process control. This work presents a sensor position FTC dedicated for PMSM, it is based on the combination of the actual

Manuscript received September 3, 2013; revised January 9, 2014; accepted January 20, 2014.
* Corresponding author: Imed JLASSI,
E-mail: imed_se@yahoo.fr
University of Tunis El Manar, LSE-ENIT B.P 37 le Belvédère 1008 Tunis, Tunisia

Copyright © JES 2014 on-line : journal/esrgroups.org/jes

sensor position and two virtual sensors (a Model Reference Adaptive System MRAS estimator and Luenberger observer). In the case of a position sensor fault, the FTC is exploited for detecting and isolating a faulty sensor for cancelling the affect of the fault and reconfigured the control scheme to a replacement the measured position error by the estimated position to ensure continuity of service without any performance degradation.

This paper is organized as follows: an introduction was given in part 1, the used control strategy of PMSM is presented in part 2, the estimator and observer design is described in part 3. Position sensor fault modeling is presented and analyzed in part 4, the proposed FTC performance is detailed in the part 5. The work and its contribution are resumed in a conclusion. Appendix and references are given.

2. Notation

The following notations are used.

V_s	Stator voltage.
$I_s(i_s)$	Stator current.
$\boldsymbol{\psi}$	Flux.
w	Rotor speed.
$\boldsymbol{\theta}$	Rotor angular position.
p	Number of pole pairs.
R_s	Stator resistance.
L_s	Stator Inductance.
J	Inertia.
f_v	Friction coefficient.
C_{em} (Cr)	Torque.
K_p, K_i	PI Controller coefficients.
L_1, L_2	Observer gain matrix.
T_S	Sampling period.

3. PMSM control design

The most common control strategies of electric drives are based on current vector control. Flux Oriented Control (FOC) is used in PMSM control. The drive is equipped with three controllers, as shown in fig.1; a direct current controller, a quadratic current controller and a speed controller. Three motor phase currents are measured by current sensors. For rotor position measurement, an incremental encoder is used. The PMSM mathematical model is developed in the (d, q) reference frame. The d component of the stator currents is forced to zero and the electromagnetic torque is controlled through the q component, in order to control the motor speed and to obtain the maximum electromagnetic torque with the minimum current. The PMSM parameters are given in table 1 of the appendix.

By the neglecting the homopolar component, the stator voltages are expressed as follows:

$$\begin{cases} V_{sd} = R_s i_{sd} + \dfrac{d\Psi_{sd}}{dt} - w_r \Psi_{sq} \\ V_{sq} = R_s i_{sq} + \dfrac{d\Psi_{sq}}{dt} + w_r \Psi_{sd} \end{cases} \quad (1)$$

The stator fluxes are given by:

$$\begin{cases} \Psi_{sd} = L_{sd} i_{sd} + \Psi_{PM} \\ \Psi_{sq} = L_{sq} i_{sq} \end{cases} \quad (2)$$

Finally the developed electromagnetic torque can be expressed as:

$$C_{em} = \frac{3}{2} p\left((L_{sd} - L_{sq}) i_{sd} i_{sq} + \Psi_{PM} i_{sq}\right) \tag{3}$$

For a Surface Permanent Magnet Synchronous Motor SPMSM (L_{sd}=L_{sq}), equation (3) can be simplified as:

$$C_{em} = \frac{3}{2}\, p\, \Psi_{PM} i_{sq} \tag{4}$$

The electromechanical equation is:

$$\frac{J}{p}\frac{dw_r}{dt} = C_{em} - f_v \frac{w_r}{p} - C_r \qquad \text{and} \qquad \frac{d\theta_r}{dt} = \Omega_r = \frac{w_r}{\mathrm{p}} \tag{5}$$

Where p is the number of pole pairs, w_r is the rotational speed and C_r is the load torque.

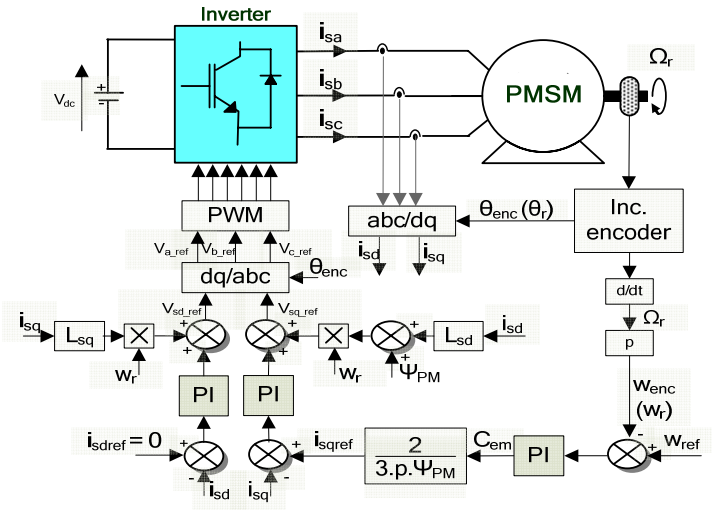

Fig.1. PMSM drive structure.

4. Estimator and Observer design

To have a strategy for the fault tolerant control FTC position sensor, we used the method based on analytical redundancy. This method using models for reconstruct information from other analytical measurement. To achieve this goal, two virtual position/ speed sensors are used; Model Reference Adaptive System MRAS estimator and Luenberger observer.

4.1. MRAS Estimator

Speed estimation methods using MRAS have been described for various works. In [15] method uses the stator flux to estimate the rotor speed for PMSG. Instantaneous and steady-state reactive power methods are used have been used to estimate the speed for a Doubly-Fed induction motor [16].

In this work, the MRAS estimator uses the stator flux to estimate the rotor speed for PMSM. The MRAS uses two models; a reference model that depends only on the stator currents to calculate the stator flux of the PMSM, the other is an adaptive model that considers the rotor speed as an adjustable parameter. The outputs of these two models are compared in an adaptation mechanism. A PI controller is used in the adaptation mechanism

to compensate the error between the two models for the convergence in the system. A bloc diagram of the proposed MRAS is shown in Fig. 2.

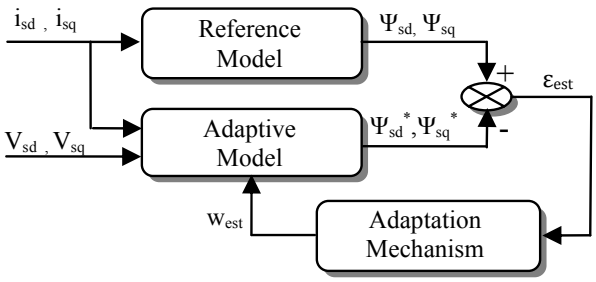

Fig.2. Structure of MRAS Estimator.

Equation (6) presents the reference model and the adaptive model is expressed as follows:

$$\begin{cases} \Psi_{sd}{}^{*} = \int \left(V_{sd} + w_{est} L_{sq} i_{sq} - R_s i_{sd}\right) dt \\ \Psi_{sq}{}^{*} = \int \left(V_{sq} - w_{est} L_{sq} i_{sd} - R_s i_{sq} + \Psi_{PM}\right) dt \end{cases} \tag{6}$$

Using (2) and (6), the adaptation mechanism is expressed as follows:

$$w_{est} = \left(K_p + \frac{K_i}{s}\right)\left(\Psi_{sd}{}^{*} \times \Psi_{sq} - \Psi_{sq}{}^{*} \times \Psi_{sd}\right) \tag{7}$$

The controller's parameters K_p and K_i are suitably chosen to assured the stability of the error ε_{est} to tune the speed estimation w_{est}.

4.2. Luenberger Observer

The main objective of the Luenberger observer is to observe the speed and the load torque from the set of stator current of the PMSM. In [11] Luenberger observer is used to observe stator and rotor currents of Doubly-Fed Induction Generator DFIG.
The derived state space model used the mechanical equation and the load torque. The load torque is supposed to be constant between two sampling time. The general state space model is given in (8), where A is the system matrix, B is the input matrix, y is the output vector and C is the output matrix. The stator current is defined as input (9) in input vector u. The rotational speed and the load torque are the states (10) in state vector x of the model.

$$\dot{x} = Ax + Bu; \qquad y = Cx \tag{8}$$

With:

$$u = \begin{bmatrix} i_{sq} & 0 \end{bmatrix}^T \tag{9}$$

$$x = \begin{bmatrix} w_r & C_r \end{bmatrix}^T \tag{10}$$

The system matrices are expressed as follows:

$$A = \begin{pmatrix} -\frac{f_v}{J} & -\frac{p}{J} \\ 0 & 0 \end{pmatrix}; \; B = \begin{pmatrix} \frac{3p^2\Psi_{PM}}{2J} \\ 0 \end{pmatrix}; \; C = \begin{pmatrix} 1 & 0 \end{pmatrix} \tag{11}$$

The state equation Luenberger observer is given in (12) and is depicted in Fig.3. The error between observed states $\hat{x}$ and measured states x is used to correct the observed states.

Error dynamics of the observer and the gain matrix L are defined by placing the eigenvalues of matrix (A-LC) to impose an observer dynamic faster than system.

$$\begin{cases} \dot{\hat{x}} = A\hat{x} + Bu + LC(x - \hat{x}) \\ \hat{y} = C\hat{x} \end{cases} \tag{12}$$

The observation error ε_{obs} and its dynamics are given by the following system of equations:

$$\begin{cases} \varepsilon_{obs} = (x - \hat{x}) \\ \dfrac{d\varepsilon_{obs}}{dt} = (A - LC)\varepsilon_{obs} \end{cases} \tag{13}$$

Where:

$$L = [L_1 \quad L_2]^T \tag{14}$$

$$(A - LC) = \begin{pmatrix} -\dfrac{f_v}{J} - L_1 & -\dfrac{p}{J} \\ -L_2 & 0 \end{pmatrix} \tag{15}$$

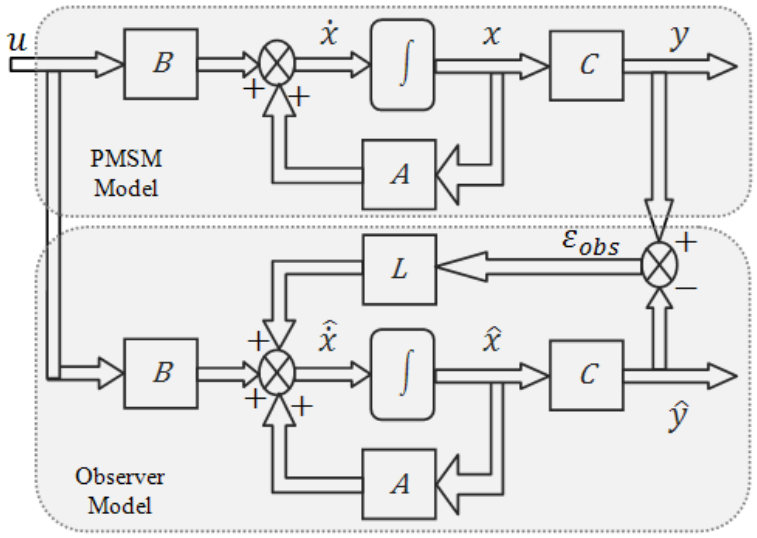

Fig. 3. Structure of the Luenberger observer.

The system is observable and observabiliy condition is verified by the following system of equations.

$$\begin{cases} det\begin{pmatrix} C \\ CA \end{pmatrix} \neq 0 \\ rank\begin{pmatrix} C \\ CA \end{pmatrix} = 2 \end{cases} \tag{16}$$

The gain matrix L_1 and L_2 are determined by resolving (17).

$$det(\lambda I_2 - (A - LC)) \tag{17}$$

Development of (17) leads to (18)

$$\lambda_{1,2} = \frac{-\left(L_1 + \dfrac{f_v}{J}\right) \pm \sqrt{\left(L_1 + \dfrac{f_v}{J}\right)^2 + 4L_2\dfrac{p}{J}}}{2} \tag{18}$$

The eignvalues system are given by

$$\begin{cases} P_1 = 0 \\ P_2 = -\dfrac{f_v}{J} \end{cases} \tag{19}$$

The eignvalues of the observer $\lambda_{1,2}$ are chosen faster than eignvalues system as expressed in (20), where n is to fix according to desired observer dynamic.

$$\lambda_{1,2} = n * P_{1.2} \tag{20}$$

Resolving (20), the gain matrix are expressed as follows

$$\begin{cases} L_1 = n * \dfrac{f_v}{J} \\ L_2 = 0 \end{cases} \tag{21}$$

The previous continuous model of the observer leads to the following discrete time state space model.

$$\begin{cases} \hat{x}(k+1) = (A_d - (LC)_d)\hat{x}(k) + B_d u(k) + (LC)_d x(k) \\ \hat{y}(k) = C\hat{x}(k) \end{cases} \tag{22}$$

Where:

$$(A_d - LC_d) = \begin{pmatrix} 1 - \left(\dfrac{f_v}{J} + L_1\right)T_s & -\dfrac{p}{J}T_s \\ -L_2 T_s & 1 \end{pmatrix} \tag{23}$$

$$B_d = \begin{pmatrix} \dfrac{3p^2\Psi_{PM}}{2J}T_s \\ 0 \end{pmatrix} \tag{24}$$

$$(LC)_d = \begin{pmatrix} L_1 T_s & 0 \\ L_2 T_s & 0 \end{pmatrix} \tag{25}$$

T_s : a sampling period.

4.3. Robustness of speed estimator and observer

It can be seen that the MRAS estimator and Luenberger observer model depend on the motor's parameters. Therefore, and to test the effectiveness of the estimator, we changed two parameters of motor Rs and Ls. Then the total stator resistance and inductance will be $R_{stot}=R_s+\Delta R_s$ and $L_{stot}=L_s+\Delta L_s$. Tests are performed at rated speed and variable load. Intensive simulations are performed under Psim and Matlab.

Fig.4 (a) shows that for variations to ΔR_s=+50% of the stator resistance or for variations to ΔL_s=-50% of the stator inductance, the speed error are negligible with the variation of load torque.

To evaluate the evolution of the eigenvalues and the dynamic of observer, we can act on inertia J. The eigenvalues of system $P_{1,2}$ and observer $\lambda_{1,2}$ are presented in Fig. 4 (b). These values have only real part with P_1=0 and P_2=-0.5215. We choose n=3, for a fast dynamic observer, then the eigenvalues of the observer are: λ_1=0 and λ_2=-1.5645. Then we evaluate

the evolution of the eigenvalues for a variation of the rotor inertia J. Therefore the total inertia will be $J_{tot}=J+\Delta J$ with $\Delta J=\pm 20\%$ of inertia J.

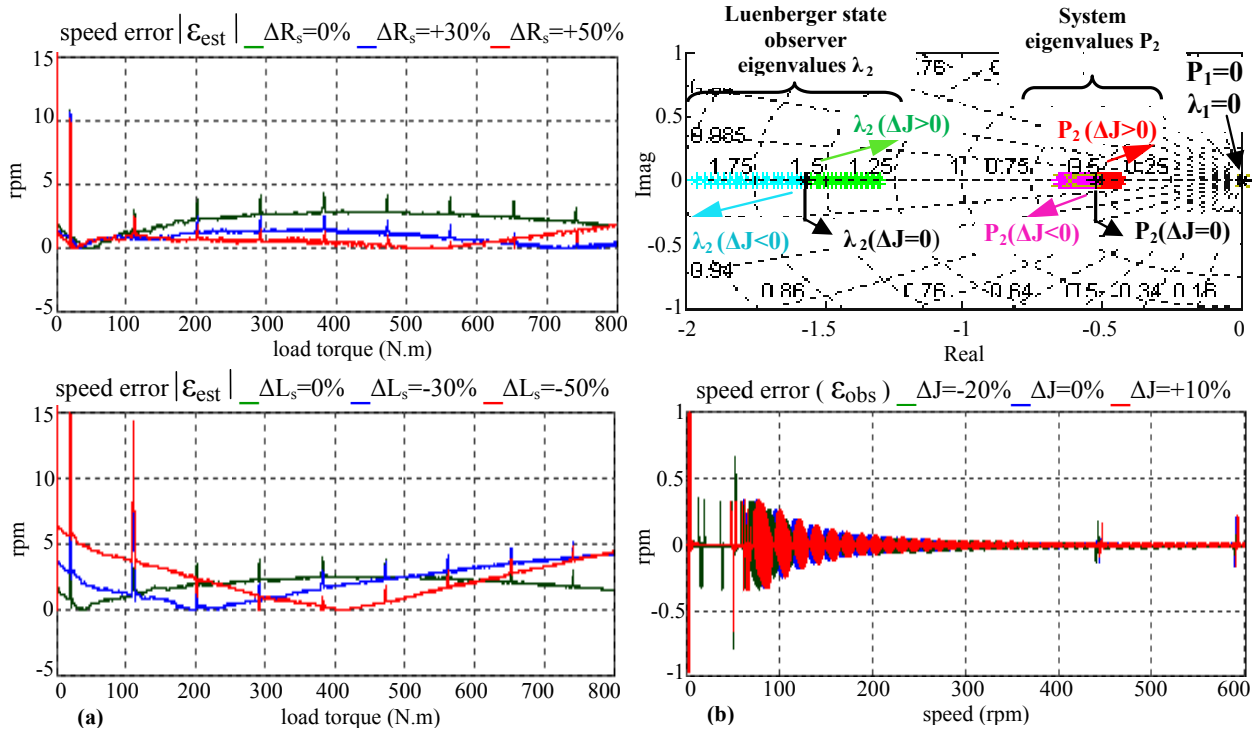

Fig.4. Robestness of the **(a)** MRAS estimator and **(b)** Luenberger observer, in case of PMSM parameters variations.

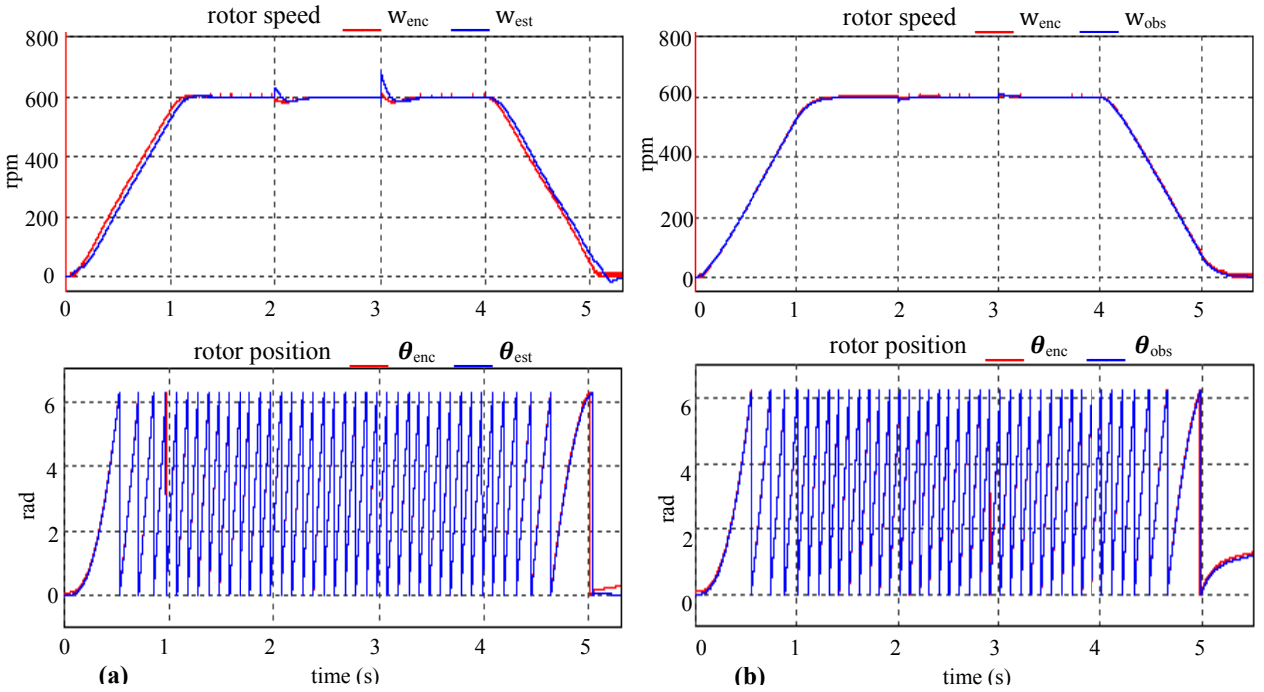

Fig.5. Speed and position in case of sensorless control using **(a)** MRAS estimator and **(b)** Luenberger observer.

It is clear that when the variation of inertia decreases gradually from 0 to -20 ($\Delta J<0$), the eigenvalues of system and observer are moving away from zero. The faster dynamic of two is achieved in this case, but the stability isn't possible. Now, if the variation of inertia

increases gradually from 0 to 20 (ΔJ>0), in this case the eigenvalues of the system and observer tend to zero. Therefore the stability is achieved but the dynamic becomes slow. Simulations are performed to evaluate the robustness of the observer, for speed and inertia variations. Fig. 4 (b) shows that, for a variation from ΔJ=-20% to ΔJ=+10%, the speed errors are negligible and are symmetrical with the variation of speed. We can conclude that the MRAS estimator and Luenberger observer reveal a good robustness.

Fig.5(a) and (b) shows the results obtained from the speed and position for position sensorless control, based on the estimator and the observer. The encoder is used for measuring the output speed. The PMSM is operated at the rated speed, the rated load is connected at t=2s and disconnected at t=3s.

It is clear that the estimator has a slow dynamic compared with the observer, during the transients, because the operation of the observer is in a close loop and he corrects the error between the real value and the observed value. But the operation of the estimator is in open loop. The results obtained show the good performances of system without position sensor. Therefore these two virtual sensors can be called to reconfigure the PMSM drive in the case of position sensor failure.

5. Position sensor fault modelling

5.1. Position sensor

In PMSM drives, an optical Incremental encoder sensor is used to determinate the rotor position. The encoder is composed of a LED, a phototransistor and a disc mounted on the motor shaft that has three tracks A, B, Z. The two tracks A and B calculate the rotor position and determine the direction of rotation. The Z track has a single hole to determine the number of turns. The principle is based on sending a light signal through the three tracks.

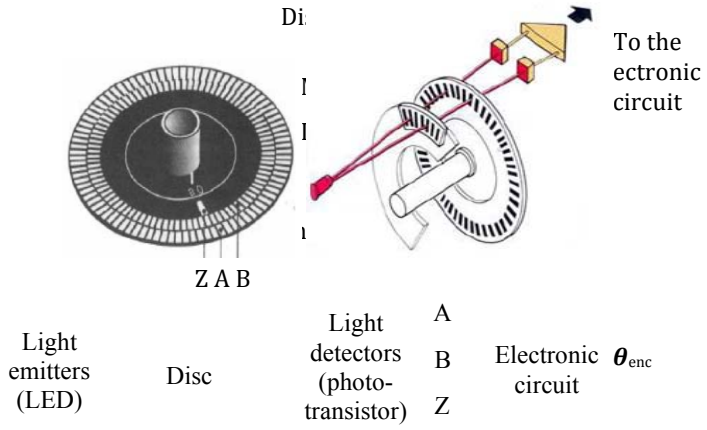

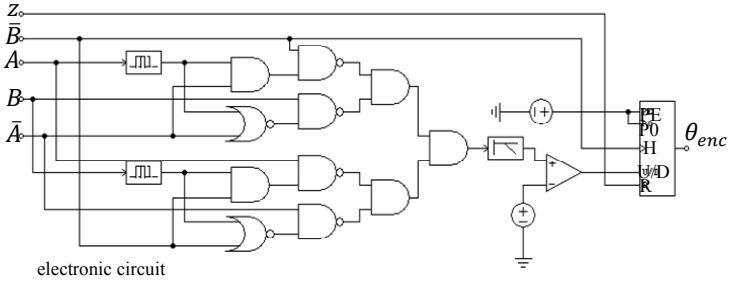

Fig. 6. Blocs diagram of the incremental encoder and electronic circuit.

The receiver is the phototransistor that converts the light pulses to binary signals 0 or 1 which correspond to a pulse dark or a pulse clear. To determine the rotor position, an electronic circuit for the recovery of the position is necessary. The structure of encoder and electronic circuit are shown in fig.6.
The block of the recovery position is composed of two elements; logical ports and a counter. The counter operates in up/down counting for each H clock pulse; if U/D=1, it increments, otherwise it decrements. The Z signal ensures the reset of counter.

5.2. Position sensor fault

The connection between the phototransistor and the electronic circuit is made from wires. It is clear that these wires are the seat of internal or external defects. The sensor can exhibit the following fault conditions:

-Loss total or partial of output information.

-Sensor gain drop.

-External disturbance.

-Offset.

In this work, a single type of incremental encoder failure is presented: a loss total or partial of output information. Indeed, a disconnection of one of these wires leads to a loss of information of the rotor position. Example, a loss of signal A or B causes loss information of direction rotation, against a loss of signal Z leads to a faulty count of position and number of rounds. The fault is applied to the signal A and the signal Z. This fault is modeled by a switch placed between the optical system and the electronic circuit. Fig.1 shows that a position sensor fault engenders an important error in Park transformation and speed controller. In this case the speed controller is not possible and the current values in the Park reference frame become erroneous.
Fig.7 (a) and (b) show the impact of position sensor fault on the speed, position and stator currents. The fault is appears at time t_d=2.59 s, when the motor operates at full load.
In the case of a signal A failure, the incremental encoder begins decrementing the position; therefore the actual position begins decrementing and the speed increases. We note that the dynamic of electrical position reconstructed by the encoder is faster compared with the mechanical position.
The signal Z failure causes the stop counting of the position, in this case the actual position decrements, which causes a drop in the speed motor. Consequently, the currents in the park reference frame become unstable and oscillating.
It is clear that a position sensor fault may seriously damage the structure of the motor drive and even causes the stoppage of the process. To limit the impact of the defect and its spread in the process, the aim is to propose a strategy for fault tolerant control FTC position sensor to detect and isolate a defect and then reconfigure the process control.

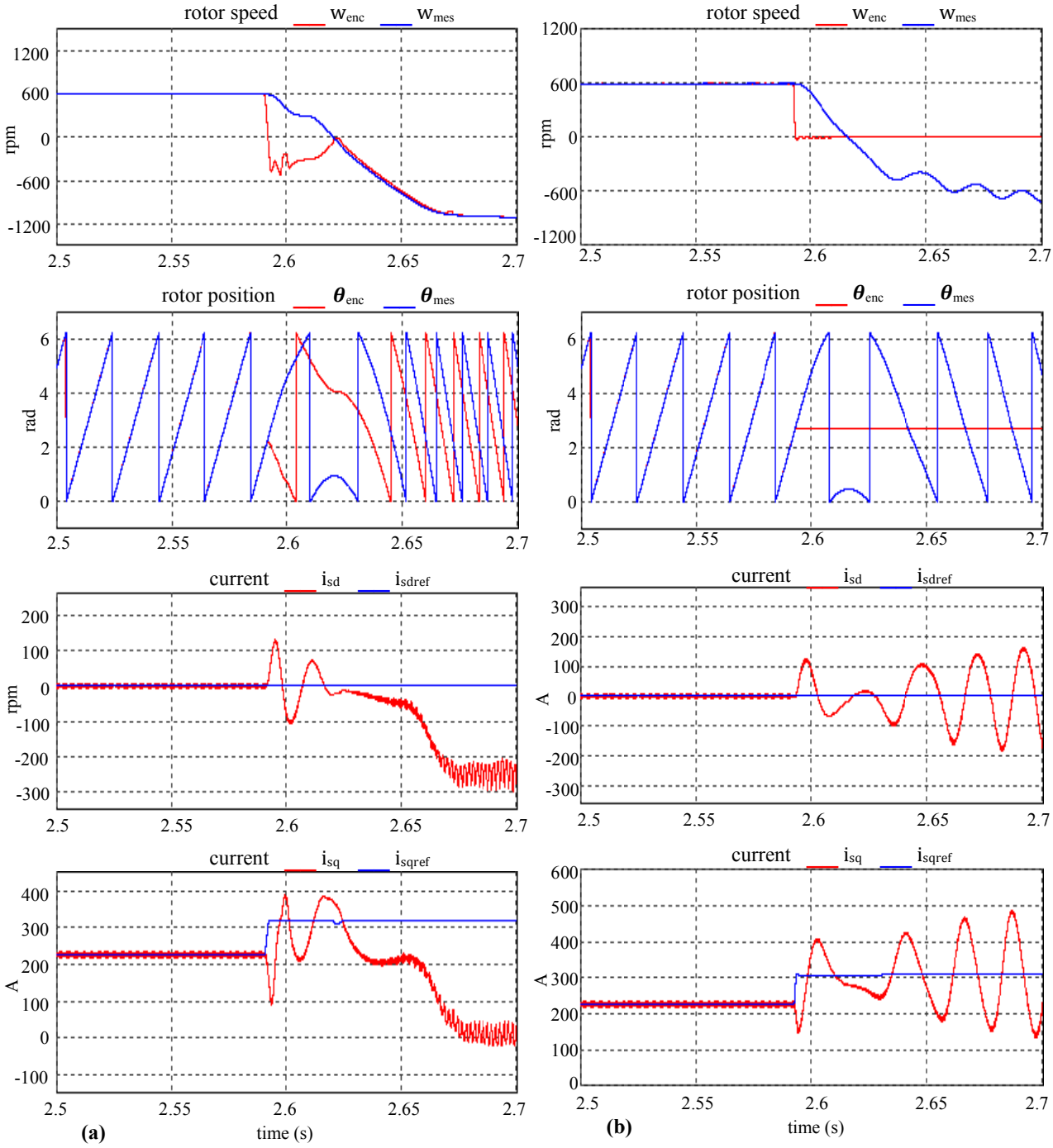

Fig.7. Simulation results in case of **(a)** signal A failure, **(b)** signal Z failure.

6. Fault Tolerant Control FTC

6.1. Position sensor fault detection

To detect the position sensor failure, we used the residues technique. The residual is a fault indicator, based on deviation between measurements and model-equation-based computations [12]. In [13] generation residual technique is used for current sensor fault detection for DFIG. This method uses measurements and observed currents to detect a fault sensor.

The technique used is based on the comparison between position/speed measured by the encoder and position/speed estimated or observed. In this case we use the MRAS estimator and Luenberger observer studied in part 3. Two residuals are used in combination to be sure of detecting the sensor fault. Residual (26) is based on the comparison between the speed measurement and the speed observed. Residual (27) is based on the comparison between the speed measurement and the speed estimation. The residuals r1 and r2 are expressed as follows:

$$r_1(t) = \frac{|w_{enc} - w_{obs}|}{w_{ref}} \times 100 \tag{26}$$

$$r_2(t) = \frac{|w_{enc} - w_{est}|}{w_{ref}} \times 100 \tag{27}$$

Fig.8 (a) and (b) shows the evolution of residues r_1 and r_2 before and after signal A and Z failure, respectively. It's clear that the residue after the fault is different to the residue before the fault; r_1 and r_2 are the magnitudes not exceeding respectively the values S_1=0.08% and S_2=2% before the defect. After the fault occurrence, the two residuals become higher than these values.

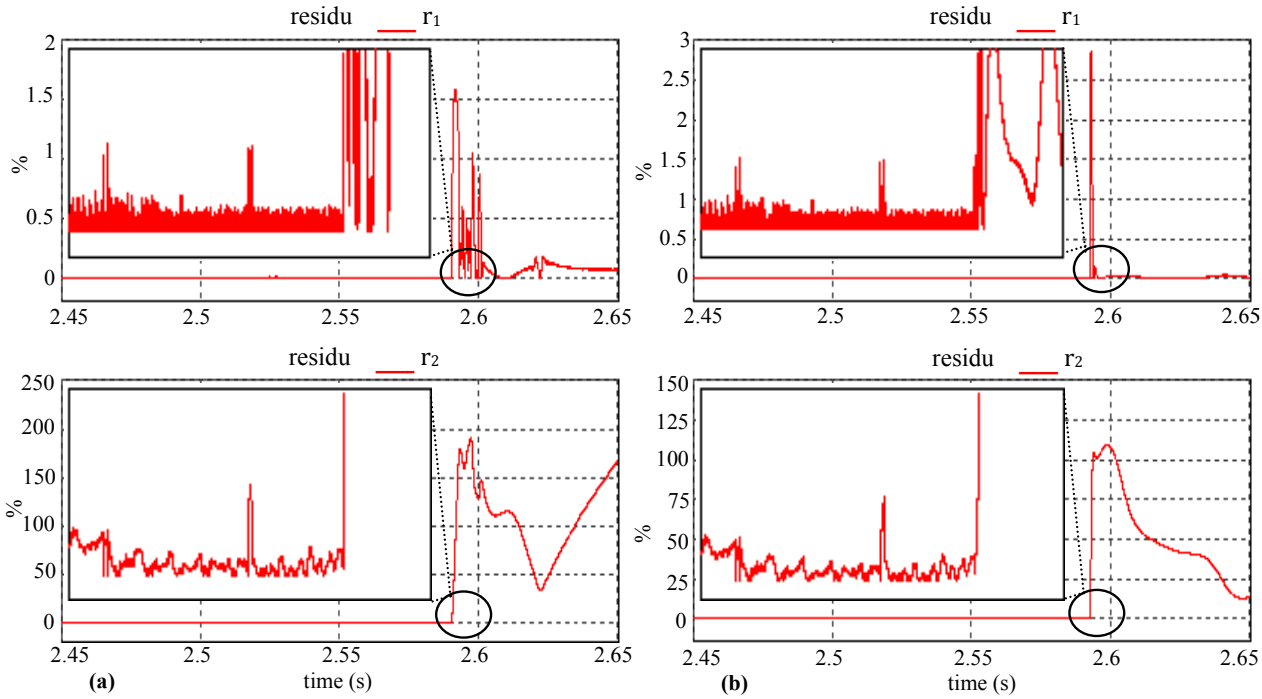

Fig.8. Residuals before and after **(a)** signal A failure, **(b)** signal Z failure.

We have developed an algorithm to enhance the diagnosis of the position sensor failure. The algorithm is based on the residues r_1 and r_2. Therefore, two fixed thresholds are used to detect the fault respectively S_1 and S_2. So, a decision signal D indicates the presence of fault when the two residues exceed their thresholds. The principle and condition of detection are resumed by (28).

$$\begin{cases} r_1(t) \geq S_1 \\ r_2(t) \geq S_2 \end{cases} \Rightarrow \quad D(t) = 1 : fault\ detected \tag{28}$$

Where: D(t) is a binary decision signal.

It is clear that the algorithm uses the two residues in combination to mention the existence of sensor failure and avoid the false alarms. If any of these conditions is false then no fault is detected and the signal D remains at zero. Fig.9 shows the structure of the detection technique.

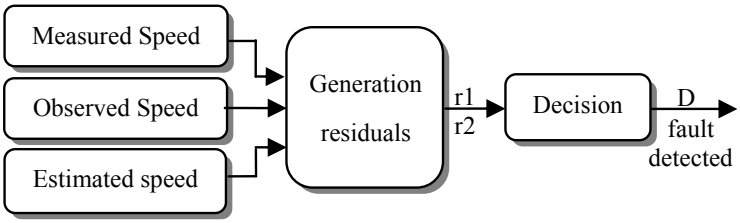

Fig.9. Technique of residual generation and detection method used.

6.2. Reconfiguration of control

After the detection, the PMSM drive is reconfigured using MRAS estimator replacement for the faulty sensor. So, the isolation of the failed sensor and the reconfiguration must be done in very short period of time, to limit the impact of the defect.

Fig.10 shows that the reconfiguration is done by the opening of the switch K_1 and closing the switch K_2 in the case of position sensor failure or intermittent sensor connection. Switching between K_1 and K_2 is achieved using the decision signal D; upon the occurrence of position sensor fault, the signal D detects this fault and sends an order to open the switch K_1 and to close the switch K_2. The switching must be done in a very short of time. The encoder will be replaced in this case by MRAS estimator in order to ensure continuity of service and maintain the system performances.

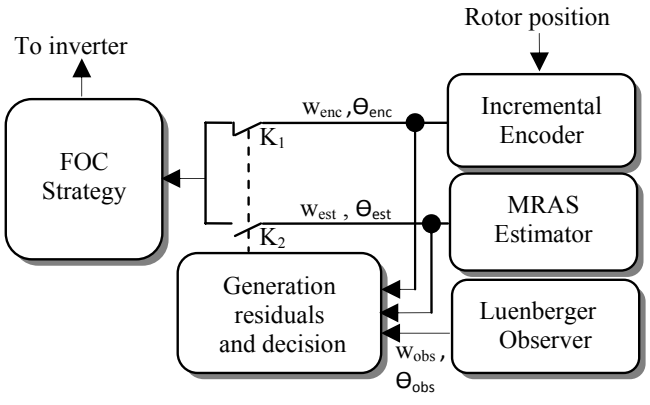

Fig.10. FTC structure.

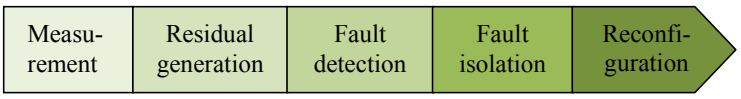

Fig.11. Necessary steps toward a fault tolerant control.

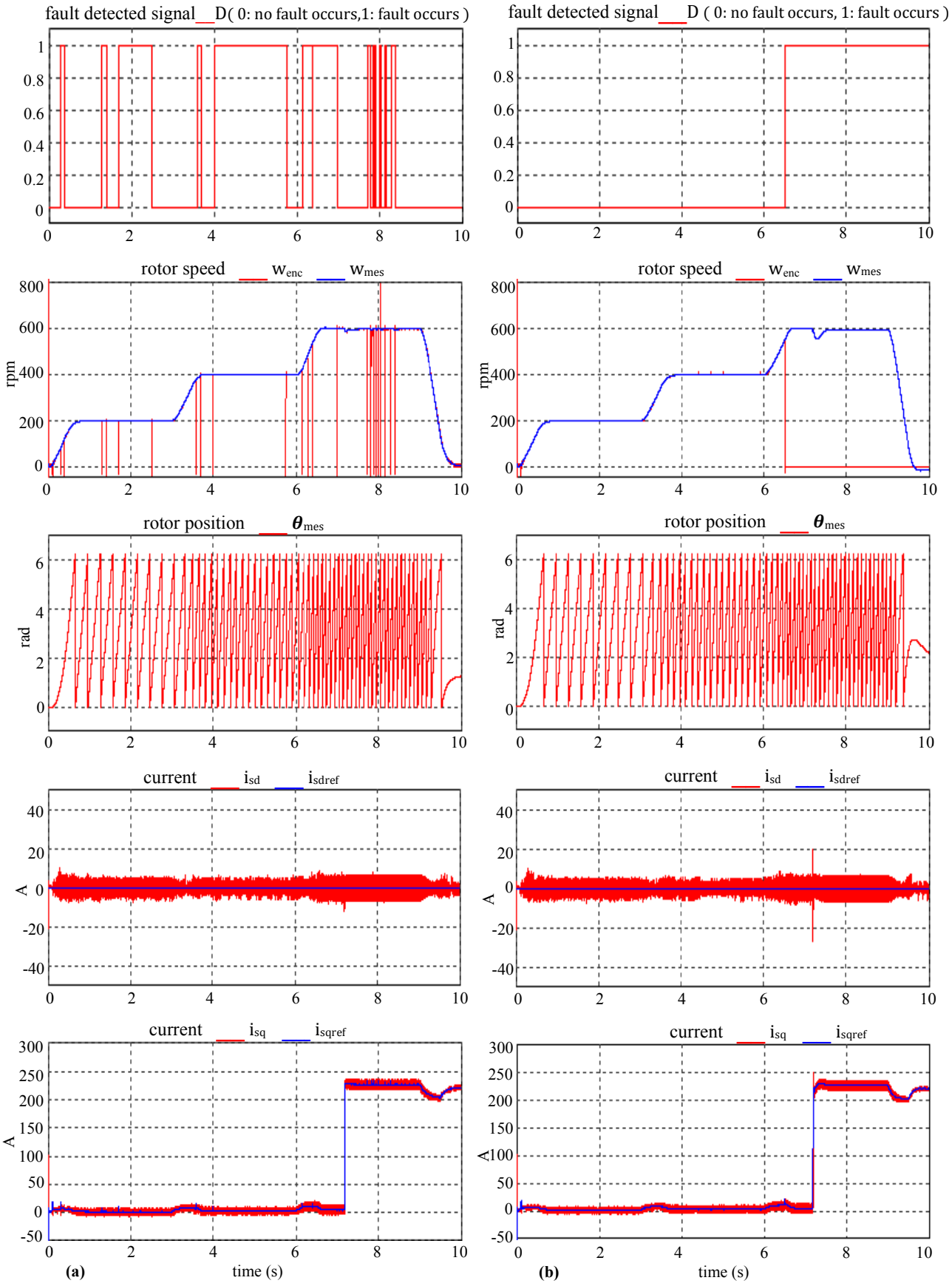

Fig.12. Reconfiguration of the system in case of **(a)** intermittent signal A connection, **(b)** permanent signal Z failure.

Then, we can resumed the steps necessary to reconfigure the PMSM drive (fig.11); the generation residuals is achieved from the measured, estimated and observed speed, to detect a position sensor fault, isolate the faulty encoder and reconfigure the PMSM drive. So, the fault tolerant control is achieved when these steps are performed.

Detection algorithm and reconfiguration method are evaluated through simulation for an intermittent signal A connection and a permanent signal Z failure. The motor operates at variable speed without load and at full load. A speed sensor is placed to give the evolution of the actual motor position $\boldsymbol{\theta}_{mes}$ and speed w_{mes} before and after the reconfiguration.

Fig.12 (a) and (b) shows that the performances of system are conserved despite the presence of the intermittent signal A failure or permanent signal Z failure. The decision signal D indicates the presence of signal A failure after a period of time Δt=0.9ms.

The signal Z failure is detected after a period of time Δt=1.2ms.

We can see that at the presence of fault, the algorithm developed scales of the measurement speed to the estimated speed. The fault is detected in a very short period of time, before the fault affects the system. Isolation and reconfiguration are in real time performed after the detection of the defect and system performances are maintained. Therefore, the position and speed keep the same form even in the existence of fault.

The current in (d, q) reference frame is the same in the case of fault and without fault. The system continues to operate in good condition, despite the existence of a faulty sensor.

These results show that the position sensor fault is limited, the reconfiguration was successful and continuity of operation is achieved.

7. Conclusion

In this work, position sensor fault tolerant control of permanent magnet synchronous motor is presented. A method based on analytical redundancy is used to detect the faulty, isolate the failed sensor, and reconfigure the control scheme. Two virtual sensors are used in combination with the PMSM drive to ensure this operation. Fault detection, isolation and reconfiguration are possible within in a very short time without interruption of drive operation. The simulation shows that the effect of fault is limited and that the performances of the motor after the reconfiguration are identical to those in safe mode.

Appendix

The PMSM parameters are listed in table1.

TABLE 1
PERMANENT MAGNET SYNCHRONOUS MOTOR PMSM PARAMETERS

Variable	Designation	Rating values
Rated power	P_n	53 kW
Pole pair	p	5
Rated speed	N_n	600 rpm
Rated current	I_{sn}	122 A
Armature resistance	R_s	87 mΩ
d-axis inductance	L_{sd}	0.8 mH
q-axis inductance	L_{sq}	0.8 mH

Acknowledgment

This work was supported by the Tunisian Ministry of High Education and Research under Grant LSE-ENIT-LR 11ES15.

References

[1] Y.K. Chin, J. Soulard, A permanent magnet synchronous motor for traction applications of electric vehicles, *3th inter. Conf. of Electric Machines and Drives, IEEE,* Vol.2, pp 1035-1041, 1-4 June 2003.

[2] J. Simanek, J.Novak, O. Cerny, R. Dolecek, FOC and Flux Weakening for Traction Drive with Permanent Magnet Synchronous Motor, *IEEE trans. Ind. Appl*., pp 753-758, 2008.

[3] Y. Zhang and J.Jiang, Bibliographical review on reconfigurable fault-tolerant control systems, *Annual Reviews in Control, ELSEVIER,* Vol.32, pp 229-252, Dec. 2008.

[4] A. Akrad, M. Hilairet, D. Diallo, Design of a Fault-Tolerant Controller Based on Observers for a PMSM Drive, *IEEE trans., Ind. Appl.,* Vol. 58, No.4, pp 1416-1427, Apr. 2011.

[5] M. Bourogaoui, H. Berriri, H.B.A. Sethom, I.S.Belkhodja, Wavelets and Parity equations methods comparison for faulty encoder detection in PMSM drives, *8th inter. Multi-Conf. on System, Signals and Devices SSD, IEEE,* pp 1-7, 22-25 Mar. 2011.

[6] Y. Jeong, S. Sul, S. Schultz, N. Patel, Fault detection and fault-tolerant control of interior permanent magnet motor drive system for electric vehicle, *IEEE trans., Ind. Appl.,* Vol.41, No.1, pp 46-51, 2005.

[7] J.S. Hu, D. Yin, and Y. Hori, Fault-tolerant traction control of electric vehicles, *Control Engineering Practice, ELSEVIER,* Vol.19, pp 204-213, Feb. 2011.

[8] D. Diallo, M. Benbouzid, A. Makouf, A fault- tolerant control for induction motor drives in automotive applications, *IEEE Trans. Veh. Technol.,* Vol.53, No.6, pp 1847-1855, 2004.

[9] M. Benbouzid, , D. Diallo, M. Zeraoulia, Advanced Fault-Tolerant Control of Induction-Motor Drives for EV/HEV Traction Applications: From Conventional to Modern and Intelligent Control Techniques, *IEEE Trans. Veh. Technol.,* Vol.56, No.2, pp 519-528, 2007.

[10] F. Zidani, M. Benbouzid, D. Diallo, A. Benchaieb, Active Fault-Tolerant Control of Induction Motor Drives in EV and HEV against Sensor Failures Using a Fuzzy Decision System, *Conf. of Electric Machines and Drives, IEMDC, IEEE,* Vol.2, pp 677-683, 1-4 June 2003.

[11] K. Rothenhagen, F.W. Fuchs, Doubly-Fed Induction Generator Model-based Sensor Fault Detection and Control Loop Reconfiguration, *IEEE trans., Ind. Appl.*, Vol.56, pp 4229-4238, 2009.

[12] K. Rothenhagen, F.W. Fuchs, Position Estimator including Saturation and Iron Losses for Encoder Fault Detection of Doubly-Fed Induction Machine, *13th Conf. of Power Electronics and Motion Control EPE-PEMC, IEEE,* pp 1390-1397, 1-3 Sept. 2008.

[13] K. Rothenhagen, F.W. Fuchs, Current Sensor Fault Detection by Bilinear Observer for a Doubly fed Induction Generator, *32nd Conf. IEEE Ind. Electronics, IECON,* pp 1369-1374, 6-10 Nov. 2006.

[14] K. S. Gaeid, H.W. Ping, M.K. Masood, L. Szabo, Survey of Wavelet Fault Diagnosis and Tolerant of Induction Machines with Case Study, *International Review of Electrical Engineering, IREE,* Vol.7,No.3, May-June 2012.

[15] J. Brahmi, L. Krichen, A. Ouali, A comparative study between three sensorless control strategies for PMSG in wind energy conversion system, *Applied Energy, ELSEVIER,* Vol.86, pp1565—1573, Sep. 2009.

[16] V. Verma, S. Maiti, C. Chakraborty, Grid-connected vector-controlled slip-ring induction machine drive without speed sensor, *Simulation and Modeling Practice and Theory, ELSEVIER,* Vol.18, pp 984-997, Aug. 2010.